Cell Stem Cell, Volume *27*

Supplemental Information

SARS-CoV-2 Infection of Pluripotent Stem Cell-Derived Human Lung Alveolar Type 2 Cells Elicits a Rapid Epithelial-Intrinsic Inflammatory Response

Jessie Huang, Adam J. Hume, Kristine M. Abo, Rhiannon B. Werder, Carlos Villacorta-Martin, Konstantinos-Dionysios Alysandratos, Mary Lou Beermann, Chantelle Simone-Roach, Jonathan Lindstrom-Vautrin, Judith Olejnik, Ellen L. Suder, Esther Bullitt, Anne Hinds, Arjun Sharma, Markus Bosmann, Ruobing Wang, Finn Hawkins, Eric J. Burks, Mohsan Saeed, Andrew A. Wilson, Elke Mühlberger, and Darrell N. Kotton

Fig. S1

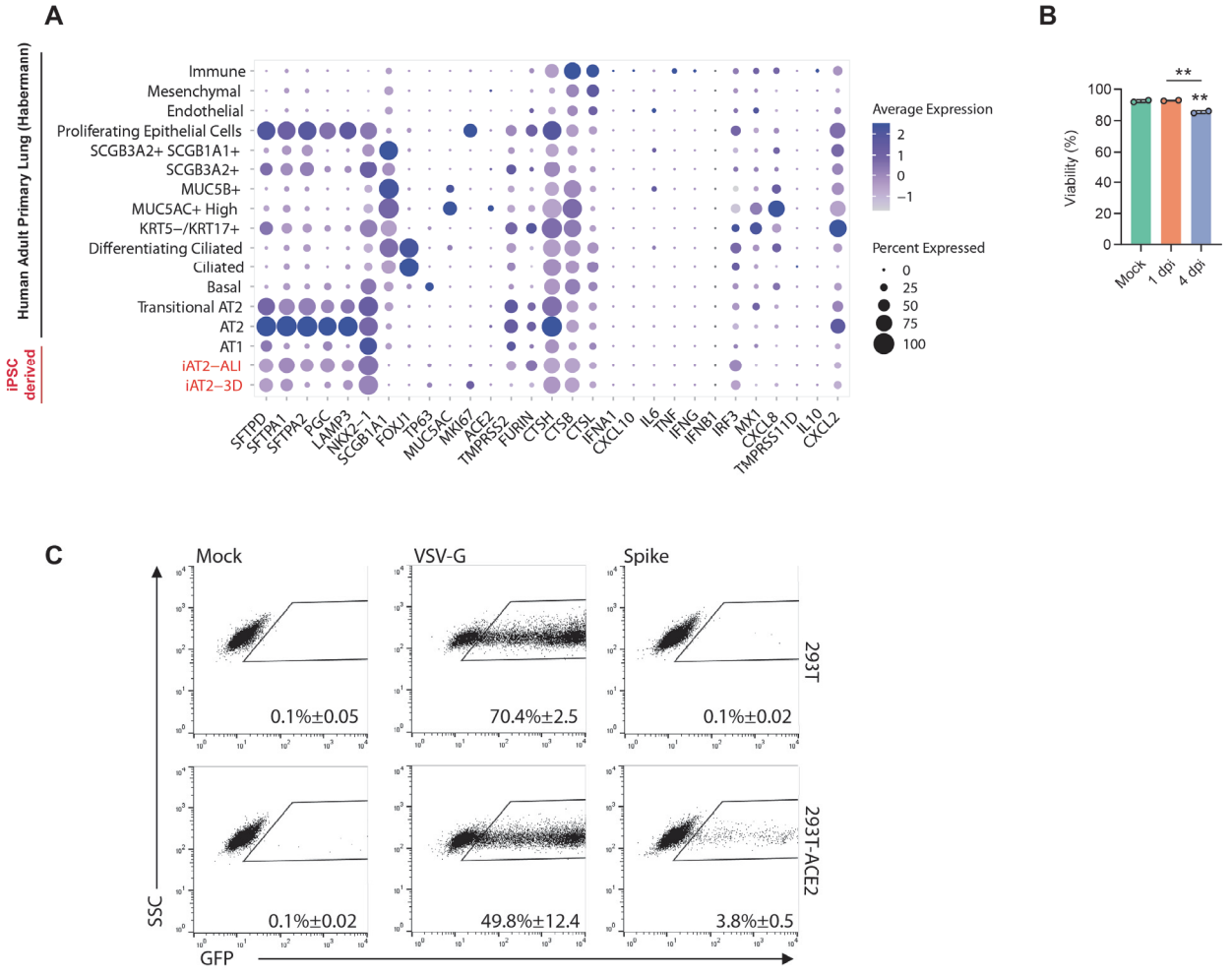

Figure S1. Single cell transcriptomic profiles of iPSC-derived vs primary lung cells, Related to Figure 1. (A) Expression of selected genes profiled by scRNA-seq in iAT2s cultured head-to-head as either 3D spheres (day 156 of differentiation) vs. 2D air-liquid interface (ALI) cultures (10 days after plating at ALI) (Abo et al., 2020). Comparison is made to a published adult primary lung epithelial dataset by Habermann (Habermann et al., 2020). Purple dot plots indicate expression frequencies and levels of transcripts associated with AT2 programs, cytokines, interferon signaling, the proliferation marker *MKI67*, or potential viral entry factors (*ACE2*, *TMPRSS2*, *FURIN*, and cathepsins B/L). (B) Percent of viable cells in mock-infected, 1 dpi, and 4 dpi samples as measured by trypan blue staining (n=2). (C) 293T and 293T-ACE2 cells were transduced with mock,VSV-G or SARS-CoV2 Spike pseudotyped GFP-expressing lentivirus. GFP+ cells were enumerated by flow cytometry (n=3).

Fig. S2

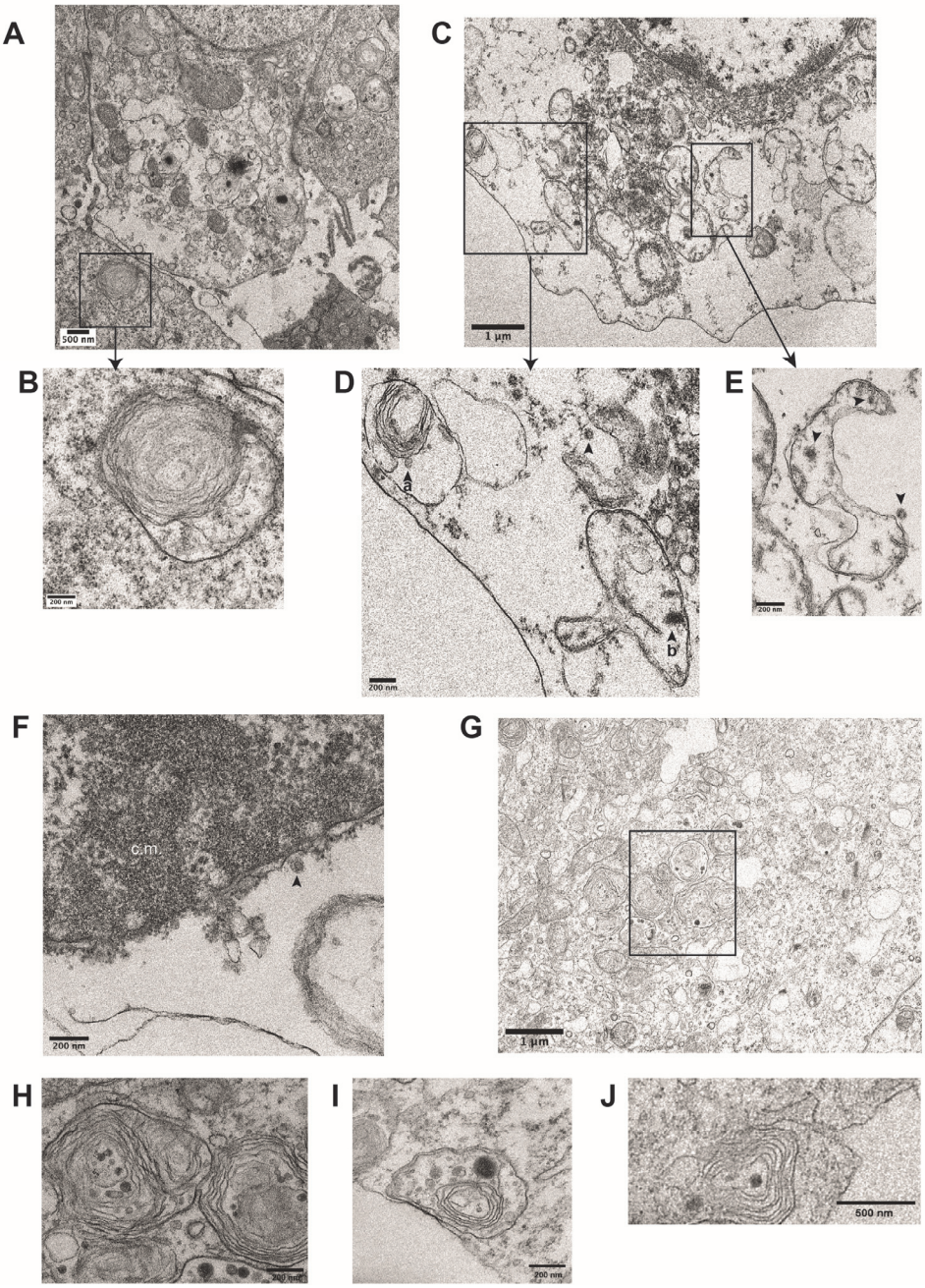

Figure S2. Ultrastructural analysis of iAT2s infected with SARS-CoV-2, Related to Figure 2. (B) Transmission electron micrographs of mock-infected iAT2s at ALI (A-B) demonstrating lamellar body expression but no detectable virions**.** iAT2s at ALI infected with SARS-CoV-2 at an MOI of 5 and fixed 1 dpi (C-G) contain visible virions (C-E, G, arrowheads) in the cytoplasm (D,E), within lamellar bodies (D, arrowhead a) (G, see Figure 2J for inset), and within double-membrane bound structures (D, arrowhead b) (E, arrowheads). Virions are also found extracellularly (F, arrowhead) and some iAT2s contain convoluted membranes (F, c.m.). (H-J) High magnification images of lamellar bodies in SARS-CoV-2-infected iAT2s.

Fig. S3

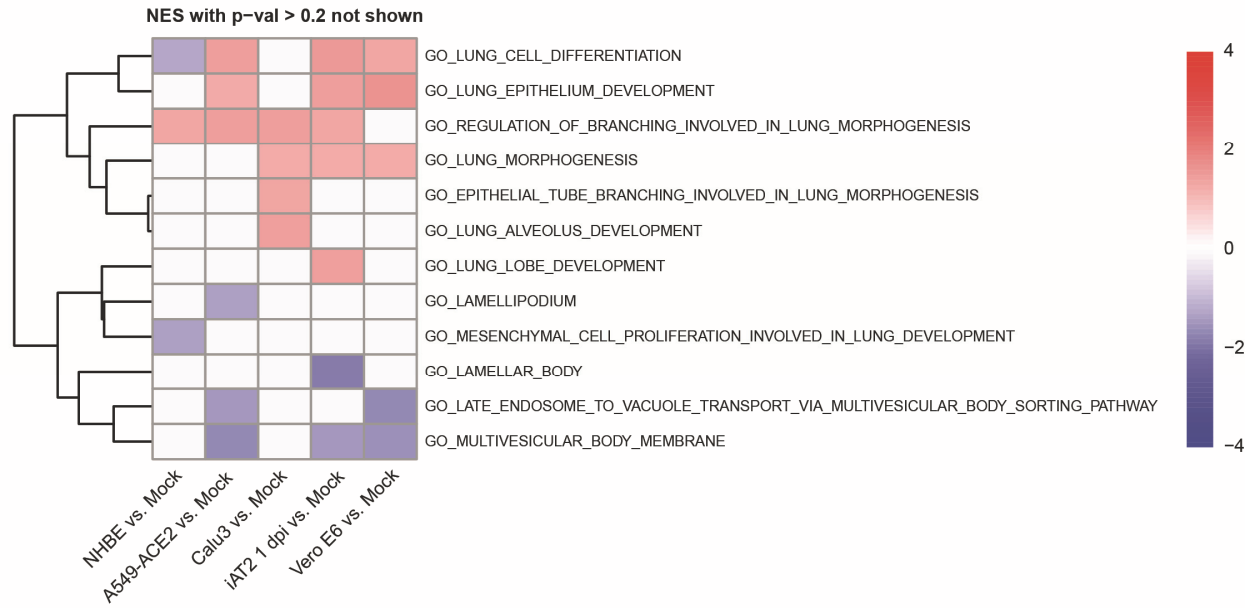

Figure S3. Functional enrichment scores on lung-related Gene Ontology terms across SARS-CoV-2 infection models, Related to Figure 3. Pre-ranked gene set enrichment analysis (FGSEA v.1.9.7) was performed on SARS-CoV-2 infected vs. mock-treated cells for 1 dpi iAT2s as well as other models systems like normal human bronchial epithelial cells (NHBE), A549-ACE2, Calu-3, and Vero E6 cells.

Fig. S4

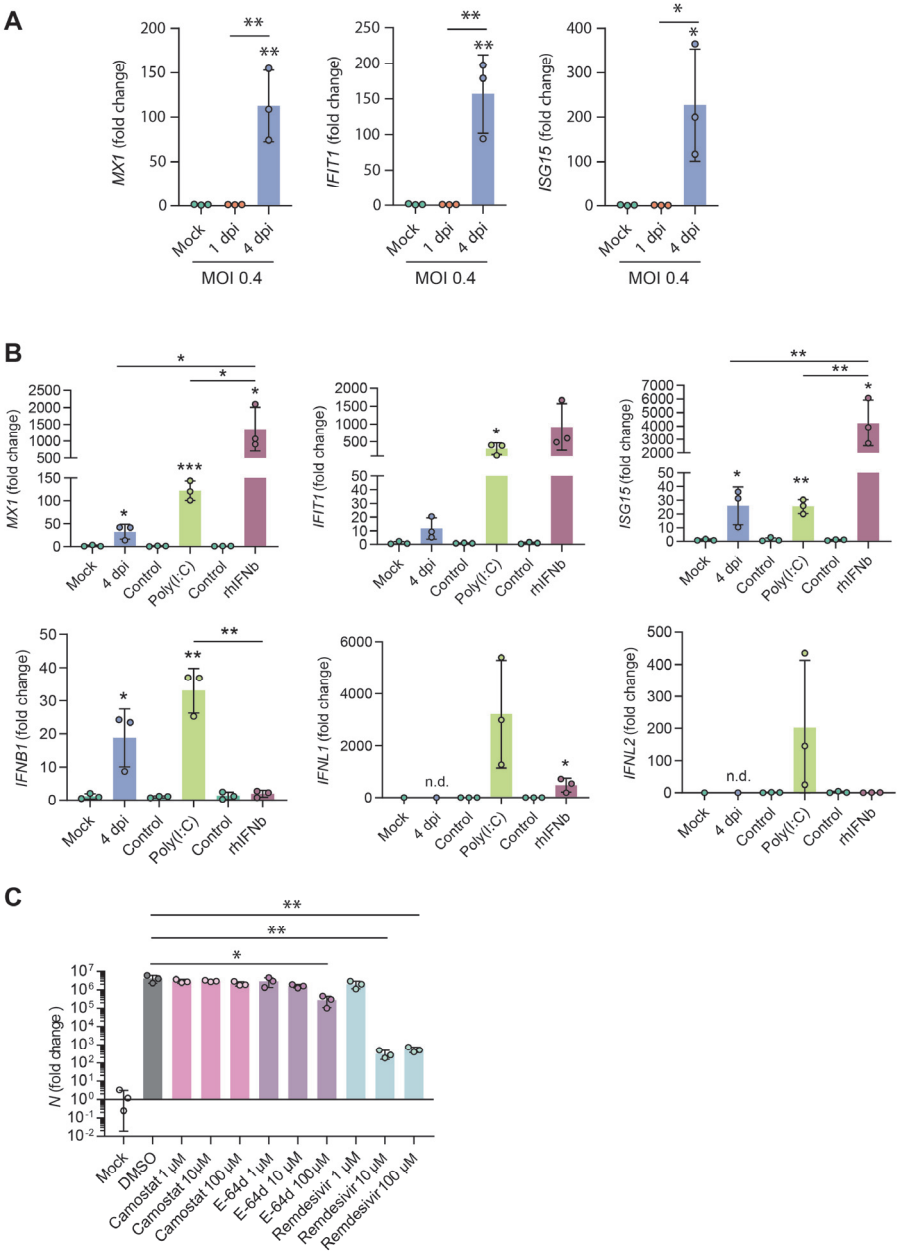

Figure S4. RT-qPCR of interferon stimulated genes (ISGs) in iAT2s and N in Vero E6 cells infected with SARS-CoV-2, Related to Figure 4. (A) Expression of ISGs in SARS-CoV-2-infected iAT2s (MOI 0.4) at 1 and 4 dpi. (B) Expression of ISGs and IFNs in SARS-CoV-2-infected iAT2s (MOI 0.4) at 4 dpi compared to 24h poly(I:C) (10 µg/mL) stimulation transfected by Oligofectamine vs. control and 24h recombinant human IFNβ (rhIFNβ, 10 ng/mL) vs. control. (C) RT-qPCR of N gene expression in Vero E6 cells at 2 dpi (MOI 0.1) with camostat (TMPRSS2 inhibitor), E-64d (cathepsin B/L inhibitor), and remdesivir treatment, n=3. All bars represent mean +/- standard deviation, n=3. *p<0.05, **p<0.01, ***p<0.001, one-way ANOVA with multiple comparisons (A, C) or unpaired, two-tailed Student's t-test (B) were performed.